



The development of functional network organization in early childhood and early adolescence: A resting-state fNIRS study

Lin Cai^{a,b,c}, Qi Dong^{a,b,c}, Haijing Niu^{a,b,c,*}

^a State Key Laboratory of Cognitive Neuroscience and Learning, Beijing Normal University, Beijing, 100875 China

^b IDG/McGovern Institute for Brain Research, Beijing Normal University, Beijing, 100875 China

^c Center for Collaboration and Innovation in Brain and Learning Sciences, Beijing Normal University, Beijing, 100875 China

ARTICLE INFO

Keywords:

Brain development
Connectome
Brain networks
fNIRS
Resting state

ABSTRACT

Early childhood (7–8 years old) and early adolescence (11–12 years old) constitute two landmark developmental stages that comprise considerable changes in neural cognition. However, very limited information from functional neuroimaging studies exists on the functional topological configuration of the human brain during specific developmental periods. In the present study, we utilized continuous resting-state functional near-infrared spectroscopy (rs-fNIRS) imaging data to examine topological changes in network organization during development from early childhood and early adolescence to adulthood. Our results showed that the properties of small-worldness and modularity were not significantly different across development, demonstrating the developmental maturity of important functional brain organization in early childhood. Intriguingly, young children had a significantly lower global efficiency than early adolescents and adults, which revealed that the integration of the distributed networks strengthens across the developmental stages underlying cognitive development. Moreover, local efficiency of young children and adolescents was significantly lower than that of adults, while there was no difference between these two younger groups. This finding demonstrated that functional segregation remained relatively steady from early childhood to early adolescence, and the brain in these developmental periods possesses no optimal network configuration. Furthermore, we found heterogeneous developmental patterns in the regional nodal properties in various brain regions, such as linear increased nodal properties in the frontal cortex, indicating increasing cognitive capacity over development. Collectively, our results demonstrated that significant topological changes in functional network organization occurred during these two critical developmental stages, and provided a novel insight into elucidating subtle changes in brain functional networks across development.

1. Introduction

Recent findings from behavioral and brain imaging studies have demonstrated that the enhancement of cognitive processes during normal brain development involves a fine-tuning of structural and functional organization of the brain from birth to adulthood (Collin and van den Heuvel, 2013; Giedd et al., 1999; Hagmann et al., 2012; Sowell et al., 2003; Vertes and Bullmore, 2015). According to Piaget's theory of cognitive development (Piaget, 1999), early childhood (7–8 years old) is a critical period during which young children undergo the transition from the preoperational stage to the concrete operational stage. Specifically, they start thinking logically about concrete events and solving problems in a more logical manner, but their thinking remains very concrete. Additionally, although numerous important cognitive functions, such as attention, memory and inhibitory control, develop

quickly, they are nonetheless less developed (Brocki and Bohlin, 2004; Davidson et al., 2006; Schneider and Ornstein, 2015). Early adolescence (11–12 years old) constitutes the starting point of the formal operational stage. In this stage, adolescents can use symbols related to abstract concepts to accomplish hypothetical and deductive reasoning, which benefits from improved working memory and executive inhibitions at this critical developmental stage (Bedard et al., 2002; Ernst and Mueller, 2008; Gathercole et al., 2004; Williams et al., 1999). These dramatic improvements of cognitive performance from early childhood to early adolescence may imply significant increases in the brain's efficiency with development. However, few studies have investigated the developmental topological characteristics of brain functional networks during these two critical periods.

The human brain constitutes an integrative, complex network system with numerous non-trivial local and global topological

* Corresponding author at: State Key Laboratory of Cognitive Neuroscience and Learning, Beijing Normal University, Beijing 100875, China.
E-mail address: niuhjing@bnu.edu.cn (H. Niu).

characteristics, which can be examined by graph theory (Bullmore and Sporns, 2009). A network's topological patterns are evaluated using the key properties of graph theory, such as clustering coefficient, characteristic path length, node degree, efficiency, and modularity (Sporns and Zwi, 2004) (see Section 2.6 for details). The clustering coefficient of a graph provides information about the level of local clustering within a graph, expressing how well the neighbors of a node are connected amongst themselves. This offers a measure of how much spatially-closer brain regions are connected with each other, or the local connectedness of the network. The level of global connectivity of the network can be assessed with the characteristic path length of a graph, which describes how close, on average, a node of the network is connected to every other node in the network. This provides information on how efficiently information can be integrated between different subgraphs. The degree of a node describes the number of connections of a node and offers information about the existence of highly connected hub nodes in the brain network. Nodes with a high nodal efficiency indicate that the network has a high tolerance for the elimination of a given node, which is associated with a high clustering of the neighborhood of this node (Achard and Bullmore, 2007). The level of modularity of a network describes the extent that groups of nodes in the graph are connected to other members of their own group, establishing sub-networks within the greater network. Taken together, these metrics of graph theory provide critical information about the structure of a network and characterize a specific organization style (e.g., small-world, modular) of that network.

Fair et al. (2009) applied resting-state functional connectivity and graph theory to investigate the topological organization of the developing brain in three age groups (aged 7–9, aged 10–15, aged 19–31). Their study revealed that children and adults have similar clustering coefficients and characteristic path lengths, but different spatial distributions of modularity organization throughout development (Fair et al., 2009). Furthermore, by comparing the organization of brain networks between 7–9 year old children and adults, Supekar et al. (2009) determined that children's and young adults' brains have a similar small-world regime, and demonstrated simultaneous reduction of short-range functional connectivity and strengthening of long-range functional connectivity from childhood to adulthood. A recent study over the age range of 6–18 years reported increases in the normalized clustering coefficient, local efficiency and small-worldness, but global efficiency was not significantly changed with development (Wu et al., 2013). The findings were further supported by a lifespan study (Cao et al., 2014) that demonstrated that local efficiency increased slightly from early childhood to early adulthood (7–30 years). To date, almost all extant literature focusing on topological developmental changes in functional networks has been performed over a relatively broad age range (Cao et al., 2014; Fair et al., 2009; Supekar et al., 2009; Wu et al., 2013). These combined results suggest that graph theoretical analysis constitutes a powerful tool to characterize the topological development of functional brain networks.

Since almost all relevant previous studies have considered a relatively wide age range, a refined examination of two relatively narrow and critical developmental periods is worthy of investigation. We predicted that the functional difference between two noncontiguous age groups will offer non-trivial insight for normal child development and a valuable reference for the clinical diagnosis of psychopathology across development. More importantly, in the current study, we adopted resting-state functional near-infrared spectroscopy (rs-fNIRS) to address the developmental changes of brain networks. Compared with functional magnetic resonance imaging (fMRI), fNIRS is silent and more tolerant to subtle movement artifacts, and can measure both oxy- and deoxy-hemoglobin chromophores, providing a more comprehensive measure of cortical hemodynamic response. Furthermore, it is generally acceptable for children to participate in fNIRS studies because data acquisition is performed in a natural environment. (Bunge and Wright, 2007; Davidson et al., 2006). In addition, compared to fMRI imaging,

fNIRS has much better temporal resolution, up to hundreds of hertz, thus providing a more complete temporal picture for the characterization of brain activity (Lloyd-Fox et al., 2010).

In the present study, we utilized rs-fNIRS to examine developmental changes in both global and regional nodal topological properties from early childhood and early adolescence to adulthood. We hypothesized that from early childhood to early adolescence, there would be a significant linear improvement in certain topological characteristics of brain networks, such as local and global efficiency, revealing functional segregation and integration. Additionally, we predicted that diverse developmental trajectories in different functional cortices would be found throughout development.

2. Materials and methods

2.1. Participants

This study enrolled 90 healthy participants, including 30 young children (age range of 7.0–8.9 years old with mean and standard deviation of 8.1 ± 0.6 years; 14 M/16 F), 30 early adolescents (age range of 11.0–12.9 years old with mean and standard deviation of 11.9 ± 0.6 years; 19 M/11 F), and 30 adults (age range of 19–27 years old with mean and standard deviation of 23.2 ± 1.9 years; 16 M/14 F). All participants were right-handed as assessed by the Edinburgh Handedness Inventory (Oldfield, 1971). The participants or their parents signed a written informed consent form prior to the initiation of the experiments. Approval for this study was obtained from the Institutional Review Board of the State Key Laboratory of Cognitive Neuroscience and Learning, Beijing Normal University.

2.2. Data acquisition

Each participant's hemodynamic response was recorded using a continuous wave near-infrared optical imaging system (CW6, TechEn Inc., MA, U.S.A.) equipped with 12 light sources and 24 detectors at 690 nm and 830 nm wavelengths. The light sources and detectors were placed on a stretchable cap, forming 46 measurement channels (source–detector separation: 3.2 cm) and covering almost the whole head (Fig. 1A, B). The positioning of the probe array was determined according to the international 10–20 coordinate system, and referred to the external auditory canals and vertex of each participant as landmarks. Specifically, six detectors below channels 17–24 in both hemispheres were set along a coronal line from the vertex to the external auditory pores, and thus their midline was localized in Cz and the leftmost and rightmost detectors were fitted around T3 and T4, respectively. Data were recorded at a sampling rate of 50 Hz. For each participant, the rs-fNIRS data were collected for approximately 11 min, and the participants were instructed to relax, keep their eyes closed, and remain awake.

2.3. MRI coregistration

To validate the positioning method of the probes, a structural MR image was acquired from one arbitrarily selected adult subject (SJ). During MRI data acquisition, the participant lay supine while wearing the probe array. The probe array was pasted with vitamin E capsules placed precisely at each of the optode locations. All scans were performed using a 3T Siemens Tim Trio MRI scanner at the Imaging Center for Brain Research, Beijing Normal University. The vitamin E locations from these scans were used as landmarks for coregistration (Fig. 1C). A T1-weighted structural image was acquired using a magnetization-prepared rapid gradient echo (MPRAGE) sequence: 176 slices, TR = 2600 ms, TE = 3.02 ms, FOV = $256 \times 224 \text{ mm}^2$, voxel size = $1 \text{ mm} \times 1 \text{ mm} \times 1 \text{ mm}$, flip angle = 8° , and slice orientation = sagittal. The MR image was normalized into MNI space using the NIRS_SPM software (<http://bispl.weebly.com/nirs-spm.html/#/>), and

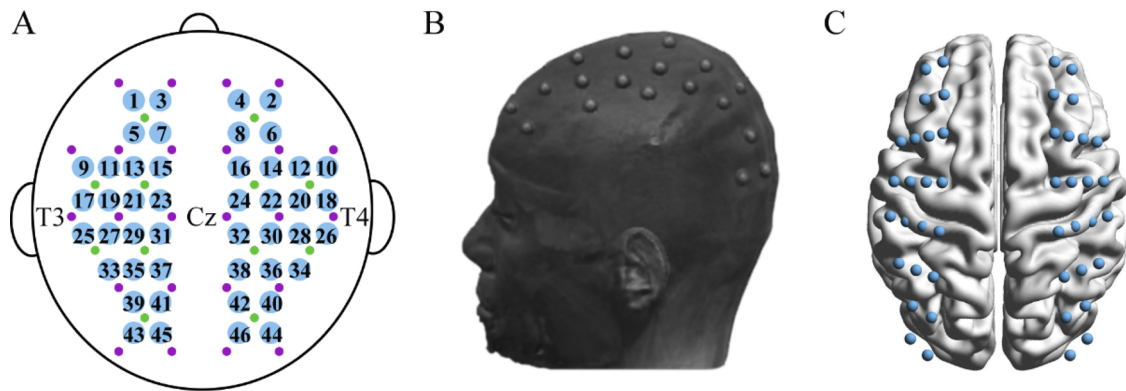


Fig. 1. fNIRS data collection and MRI Neuroanatomical Co-Registration. (A) The arrangement of the 46 measurement channels across the whole head. The green and purple dots represent the sources and detectors, respectively. The digits represent the positions of the measurement channels. (B) MRI co-registration was conducted by asking a participant to wear probe arrays with vitamin E capsules in MRI. (C) The anatomical position corresponding to each measurement channel. (For interpretation of the references to colour in this figure legend, the reader is referred to the web version of this article.)

the Montreal Neurological Institute (MNI) coordinates for each measurement channel were determined according to the automated anatomical labeling (AAL) template (Tzourio-Mazoyer et al., 2002). A similar positioning method can be found in previous fNIRS studies (Kovelman et al., 2008; Kovelman et al., 2009; Sasai et al., 2012). For the cortical position corresponding to each measurement channel, see Table S1 in Supplementary Materials.

2.4. Data preprocessing

We evaluated the relative changes in oxy-hemoglobin (HbO) and deoxy-hemoglobin (HbR) concentration on an arbitrarily assigned zero baseline from the start of the measurement period, which was based on the modified Lambert–Beer law (Cope and Delpy, 1988). For the time course of the HbO and HbR signals, we first conducted a temporal independent component analysis (ICA) to remove typical motion-induced artifacts and systematic physiological noise (Niu et al., 2013). This analysis procedure was performed by using a publicly available software, *FastICA* v2.5 (www.cis.hut.fi/projects/ica/fastica/). Specifically, the ICA analysis was separately performed on the raw data of HbO and HbR with the following procedures: 1) extracting steady hemoglobin concentration signals (i.e., removing the initial time points from total data length); 2) reducing the dimensionality of the data with principal component analysis; 3) performing ICA analysis on the reduced dimensional data; 4) identifying noise components; 5) removing noise from the measured data and calculating “real” neural activity signals. After ICA analysis, the components related to motion-induced artifacts and physiological noise were identified from three aspects: temporal profiles, spatial maps, and power spectra. A component was treated as noise if it met one of the following criterion (Zhang et al., 2010): 1) the corresponding temporal profile included sudden jumps, slowly varied U or inverted U-shaped spike, or numerous inter-current quick spikes; 2) the dominant frequency of power spectra of the component was outside the range of 0.01–0.1 Hz; or 3) the spatial map of the component presented a global and spatially dispersive pattern. After identifying these types of noise components, each concentration signal of HbO and HbR was reconstructed with a particular component eliminated from the original rs-fNIRS time course by replacing zero in the corresponding column of the mixing matrix (Kohno et al., 2007). Then, we adopted a band-pass filtering with cutoff frequencies of 0.009 and 0.08 Hz to reduce the effect of high-frequency noise and baseline drift, and to obtain the low frequency hemodynamic signals that emanated from spontaneous neural activity (Biswal et al., 1995; Sasai et al., 2012; White et al., 2009). Finally, we extracted 10-min data, including 30,000 sample points, from the continuous time course of each participant to perform the network topology analyses. The data preprocessing was conducted using in-house FC-NIRS package (<http://www.nitrc.org/>

[projects/fcnirs](http://www.nitrc.org/projects/fcnirs/); Xu et al. (2015)), which was developed using MATLAB 2010b (www.mathworks.org) in a 64-bit Windows 7 environment. In the current study, we mainly used HbR signals to characterize topological development of functional brain networks, considering that HbR has been demonstrated in our previous study (Niu et al., 2013) to have an overall much higher reliability for most brain network metrics and consistently considered as the physiological basis of the fMRI BOLD signals (Buxton et al., 1998; Ogawa et al., 1993). The brain development results derived from the HbR signals also allow us to make a direct comparison with those derived from fMRI. As a complement, HbO signals were also utilized in our study to investigate the topological development of functional brain networks. The HbO results were included in the Supplementary Materials.

2.5. Network construction

The application of graph theory to construct human brain functional networks extracted from functional imaging data requires two steps to be performed. First, the nodes should be defined. Second, the strength of the connections between any two nodes needs to be quantified by similarity measures (e.g., Pearson correlation) between their respective time series above a threshold. If the strength of the connections exceeds the predefined threshold, the connections are treated as the edges of a graph. These two steps are important since the definition of the nodes and the edges determines the network properties that are then used for neurobiological interpretation (Rubinov and Sporns, 2010). Commonly applied thresholding methods include correlation-based and sparsity-based methods. Correlation-based method generally sets a value for the correlation coefficient between node pairs, above which they are considered connected and below which they are not. This method will result in different numbers of edges due to differences in the low-level correlations among different groups. In contrast, sparsity-based thresholds generally define network sparsity as the ratio of the number of existing edges divided by the maximum possible number of edges in a network. For group comparisons, this method can ensure that the networks have the same number of edges or wiring cost for each group (Achard and Bullmore, 2007; Stam et al., 2007). Therefore, in the current study, we adopted the sparsity-based method to construct brain network and then to conduct group comparison of topological development of brain networks.

In the current study, we used MATLAB (www.mathworks.org) functions from the GRETNA toolbox (<http://www.nitrc.org/projects/gretna>; Wang et al., 2015) to construct the brain functional network for each subject. For each individual rs-fNIRS data set, we obtained a 46×46 symmetric correlation matrix by calculating Pearson correlation coefficients between the time series of every pair of nodes in which the nodes were the measurement channels. Due to the ambiguous

biological explanation of negative correlations (Fox et al., 2009; Murphy et al., 2009), we replaced all negative correlation coefficients to zero and restricted our analysis to positive correlations. These correlation coefficients were then converted to Z-values via Fisher’s *r*-to-*z* transformation to improve normality, resulting in a 46×46 Z-value functional connectivity matrix Z_{ij} for each subject, where $i, j = 1, 2, \dots, 46$. Each functional connectivity matrix can be converted to a binarized B_{ij} using a sparsity threshold, where B_{ij} is 1 if the value of the Z-value functional connectivity matrix Z_{ij} between regions i and j is larger than a given sparsity threshold, and 0 otherwise. To perform a group-averaged functional connectivity comparison, the individual Z-value functional connectivity matrices were first averaged within each age group, and then the group-level Z-value matrix was converted into an R-value matrix via Fisher’s *z*-to-*r* transformation for each age group, respectively. Of note, the main network analyses were based on binary brain networks. However, the effects of other sparsity thresholds and weighted network analysis on our results were also evaluated (see the following Section 2.8 “Validation”).

2.6. Network analysis

Graph theory was utilized to describe the topological organization of the human brain functional networks. Similar to earlier studies (Bassett et al., 2008), the correlation matrix was thresholded over a range of sparsity ($5\% < s < 25\%$, stepsize = 1%) in order to investigate the relationship between sparsity and the network properties. Meanwhile, we also adopted a single sparsity ($s = 20\%$) to normalize all of the networks to have the same number of edges, and thus to explore the between-group differences in the same-size network topological organization. These network metrics are explained as follows:

2.6.1. Global network metrics

Six global network metrics, including the normalized clustering coefficient (C_p), characteristic path length (L_p), global efficiency (E_{glob}), local efficiency (E_{loc}), small-worldness (σ), and modularity (Q) were used to elucidate global topological organizational changes in the developing brain (for illustrations, see Fig. 2) (Fair et al., 2009; Fan et al., 2011). Their definitions and descriptions can be found as follows, and in Rubinov and Sporns (2010).

For graph G with N nodes and K edges, the clustering coefficient C_p of the graph G is calculated as follows (Watts and Strogatz, 1998):

$$C_p = \frac{1}{N} \sum_{i \in G} \frac{E_i}{D_i(D_i - 1)/2}$$

where D_i denotes the number of edges connected to node i ; and E_i is the number of edges in the subgraph, including the neighbors of node i . The clustering coefficient reflects the local interconnectivity and cliquishness of a network.

The characteristic path length L_p of graph G is defined as the

average of the shortest path lengths between all pairs of nodes in network G (Watts and Strogatz, 1998):

$$L_p = \frac{1}{N(N - 1)} \sum_{i \neq j \in G} d_{ij}$$

where d_{ij} is the shortest path length between node i and node j . The shortest path length is the minimum number of edges included in the path that connected these two nodes. The characteristic path length measures the ability of parallel information propagation (Latora and Marchiori, 2003).

To examine the small-world attributes of a network, the normalized clustering coefficient $\gamma = C_p^{real}/C_p^{rand}$ and the normalized characteristic path length $\lambda = L_p^{real}/L_p^{rand}$ were computed (Watts and Strogatz, 1998). C_p^{real} and L_p^{real} are the clustering coefficient and the characteristic path length of a real network, respectively, and C_p^{rand} and L_p^{rand} represent the means of the corresponding parameters derived from 1000 matched random networks that have the same numbers of nodes, edges, and distribution of degrees as the real brain network. Typically, a small-world network should meet the following criteria: $\gamma > 1$ and $\lambda \approx 1$ (Uehara et al., 2014).

In addition to the conventional small-world parameters (C_p and L_p), the more biologically relevant properties of brain networks are efficiency parameters, including global efficiency and local efficiency, which measure the capability of the network with regard to information transmission at the global and local levels, respectively. Global efficiency E_{glob} is defined as the inverse of the harmonic mean of the shortest path length between any two nodes (Latora and Marchiori, 2001):

$$E_{glob} = \frac{1}{N(N - 1)} \sum_{i \neq j \in G} \frac{1}{d_{ij}}$$

where d_{ij} is the shortest path length between node i and node j .

Local efficiency E_{loc} of a network G is defined as the average of the local efficiencies of all nodes, where the local nodal efficiency for a given node i is the global efficiency of the subgraph composed of the nearest neighbors to node i (Achard and Bullmore, 2007; Latora and Marchiori, 2001):

$$E_{loc} = \frac{1}{N} \sum_{i \in G} E_{glob}(i)$$

where $E_{glob}(i)$ is the global efficiency of G_i , which is the subgraph of the neighbors of node i . The use of global efficiency is more advantageous than the use of the characteristic path length, particularly in the case of disconnected networks, because the disconnected nodes are considered to have an infinite path length and a corresponding zero efficiency.

Modularity reflects the degree to which a network is organized into a modular or community structure (Newman, 2006). For a given partition p of a network, the modularity is defined as follows:

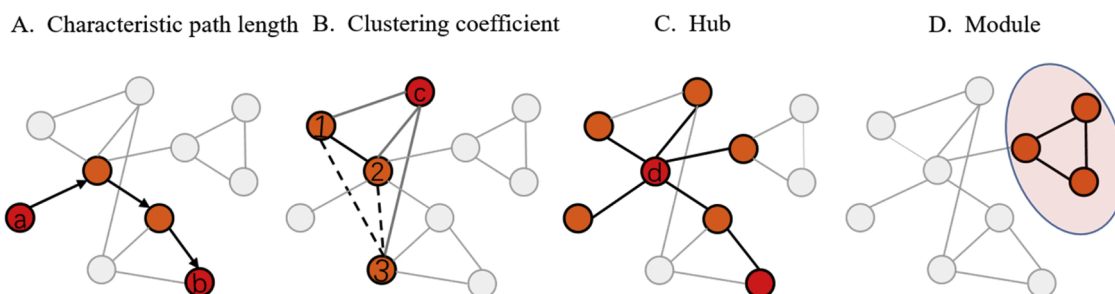


Fig. 2. The topological properties of networks. We illustrate the topological properties of networks by a network composed of 10 nodes and 13 edges. (A) The characteristic path length between nodes a and b is the shortest path length, as indicated by the three black arrow lines. (B) The clustering coefficient of node c is the number of existing connections (i.e., 1–2) among the node’s neighbors divided by all of their possible connections (i.e., 1–2, 1–3, 2–3), which is 1/3 (the dashed lines indicate the absence of a connection between the neighbors of node c). (C) Shows a network with a highly connected hub node d, which plays a central position in the overall network. (D) Shows the presence of a clustered module, as indicated by the three nodes (encircled in pink) being mutually strongly interconnected, but sparsely connected to the rest of the network.

$$Q(p) = \sum_M^{m-1} \left[\frac{l_m}{L} - \left(\frac{d_m}{2L} \right)^2 \right]$$

where M is the number of modules; L is the number of connections in the network; l_m is the number of connections between the nodes in module m ; and d_m is the sum of the degrees of the nodes in module m . The modularity attempts to partition the graph into disconnected subgraphs to minimize the degree of inter-module connectivity and maximize intra-module connectivity.

2.6.2. Regional nodal metrics

Regional topological characteristics were evaluated in terms of nodal degree and nodal efficiency. The degree of a given node i is defined as the number of edges linked to the node as:

$$K_{nod}(i) = \sum_{j \neq i \in G} a_{ij},$$

where a_{ij} is the i^{th} row and j^{th} column element in the formerly obtained adjacency matrix.

The efficiency of node i is measured as follows:

$$E_{nod}(i) = \frac{1}{N-1} \sum_{j \neq i \in G} \frac{i}{d(i, j)},$$

where $d(i, j)$ is the shortest path length between node i and node j . Nodes with a high nodal efficiency indicate that the network has a high tolerance to the elimination of a given node, which is associated with a high clustering of the neighborhood of this node (Achard and Bullmore, 2007). In addition, we employed nodal degree and nodal efficiency to identify functional hubs across three age groups, respectively. The nodes with higher values in nodal degree and nodal efficiency (at least 1 standard deviation greater than the average of all nodes in the network) were defined as brain hubs, which are usually assumed to play central roles in the functional integrity of whole brain networks. BrainNet Viewer (<http://www.nitrc.org/projects/bnv/>) was used for visualization of regional nodal properties.

2.7. Statistical analysis

To characterize the developmental changes in global topological properties, we separately performed one-way analysis of variance (ANOVA) on the three age groups for each global metric. Tukey's honest significant difference (HSD) tests were applied as *post hoc* tests. Furthermore, to guarantee the statistical reliability of the obtained findings, a bootstrap analysis of the confidence intervals was conducted using 1000 bootstrap samples. For the global network properties, confidence intervals (95%) for each topological property among these three age groups were calculated from the bootstrap values, and the differences among the groups were determined by the lack of overlap in these confidence intervals (Garrett et al., 2013).

To determine the developmental changes in regional nodal properties from early childhood, early adolescence to adulthood, a general linear model (GLM) was utilized for each nodal metric. Specifically, to explore linear or quadratic age effects, we used two multiple linear regressions that modeled each nodal metric with age or age² as predictors. The GLM models were separately formulated as follows:

$$Y = \beta_0 + \beta_1 \times \text{age} + e$$

$$Y = \beta_0 + \beta_1 \times \text{age} + \beta_2 \times \text{age}^2 + e$$

We adopted a finite sample corrected Akaike's information criterion (AIC), namely, AICc (Hurvich and Tsai, 1989), to determine the best model among the two regressions. AIC reflects a trade-off between the likelihood and complexity (i.e., number of parameters) of a model. The regression model with the lowest AICc value was chosen as the best model to fit the data. Multiple comparisons among channels were considered by adopting Bonferroni correction for HbO data and the

false discovery rate (FDR) correction at $q < 0.05$ (Benjamini and Hochberg, 1995) for HbR data.

2.8. Validation

Considering that network sparsity thresholds and different network construction approaches may influence the reproducibility of the network topological attributes derived from the rs-fNIRS data, we performed additional complementary analyses. On the one hand, we recomputed the developmental changes in the global topological properties and regional nodal properties using two other sparsity thresholds (i.e., 15% and 25%) and then performed the statistical analyses. On the other hand, weighted networks were computed to validate the reproducibility of our results. Moreover, we also used HbO signals to examine the effect of different hemoglobin concentration signals on our main results.

3. Results

3.1. Functional connectivity

We showed the functional connectivity pattern at the group level for young children, early adolescents, and adults, respectively (Fig. 3). We determined that the functional connectivity correlation coefficients in young children (mean \pm SD = 0.23 \pm 0.01) and early adolescents (mean \pm SD = 0.18 \pm 0.01) had a shorter tail of positive correlations compared to those in the adult group (mean \pm SD = 0.13 \pm 0.02). Young children and early adolescents also exhibited similar functional connectivity organization as that in adults, i.e., high correlations between the contralateral homologous regions and the neighboring ipsilateral regions.

3.2. Economic small-world organization

Fig. 4 shows the profiles of six global parameters calculated from both the real brain network (warm colors) and random networks (cold colors), and shown as functions of the sparsity thresholds. We found that in the sparsity range of 5% ~ 25%, the C_p values of brain functional networks were larger than those of the matched random networks (Fig. 4A), and the L_p values were comparable to those of the matched random networks (Fig. 4B). When evaluating the small-worldness, we observed that the small-worldness values were larger than 1 in the sparsity range of 5% ~ 25% in all three age groups (Fig. 4C). Thus, these network organizations for each age group reflect typical features of small-world topology, demonstrating a balance between local segregation and global integration in the developing brain. From the perspective of the efficiency, the local efficiency of the networks was larger than that of the matched random networks (Fig. 4E), whereas the global efficiency of the networks was comparable to that of the matched random networks (Fig. 4D). These results further supported the small-worldness organization of the brain networks, which are approximately efficient in global information processing, but more efficient in local information processing compared with the matched random networks. Furthermore, the functional brain networks in these three age groups consistently showed a higher modularity compared with that derived from the matched random networks (Fig. 4F). These combined results demonstrated that functional brain connectivity networks in young children and early adolescents have been specially organized according to non-trivial wiring principles.

3.3. Developmental changes in global network properties

One-way ANOVAs were utilized to conduct the developmental comparison in network topological measures among the age groups. With development, significant age effects were found on the normalized C_p ($F_{(2,87)} = 5.15$, $p = 0.008$), small-worldness ($F_{(2,87)} = 3.45$,

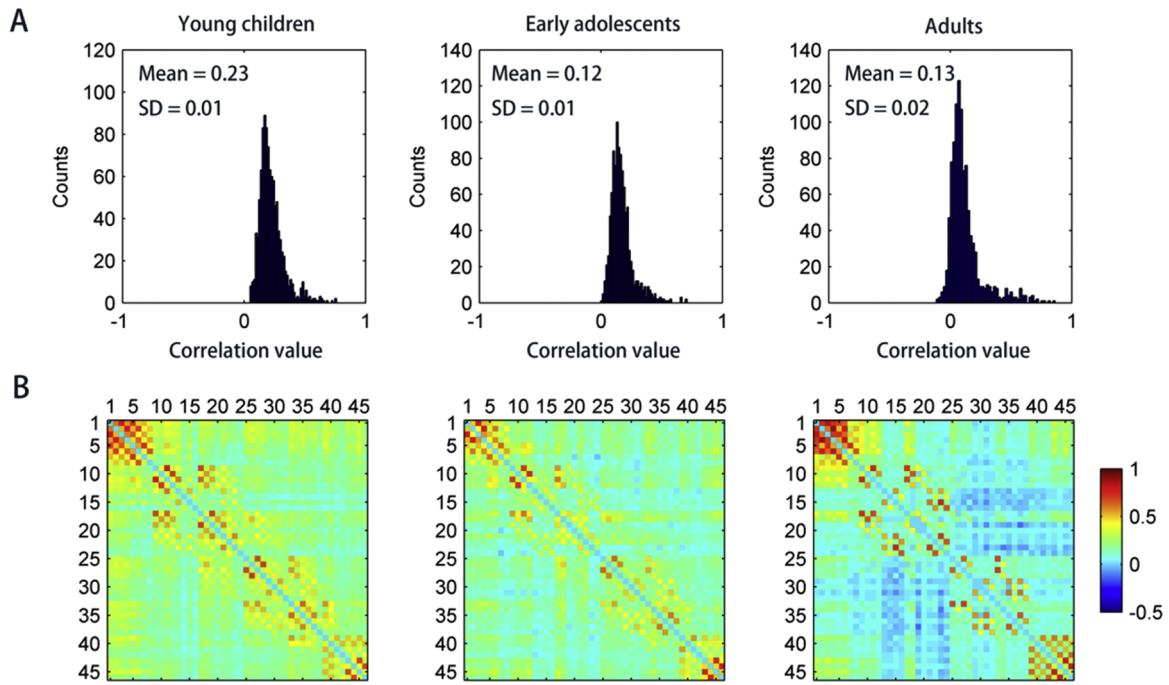


Fig. 3. The distribution of r values within the raw r value correlation matrices of three age groups (A). The averaged population-level correlation matrices of three age groups (B) (digits in matrices represent measurement channels).

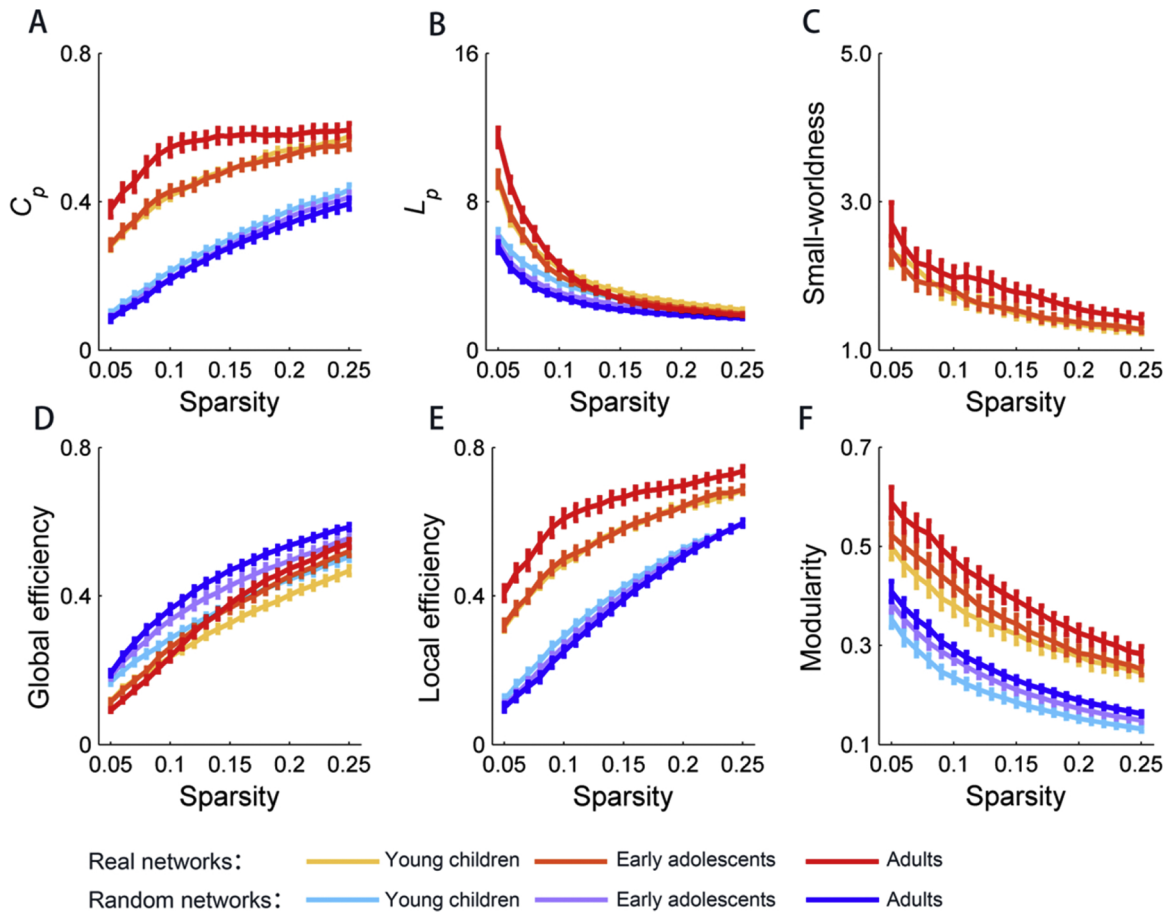


Fig. 4. The global network metrics in a range of sparsity thresholds (5%–25%). (A) The clustering coefficient and (B) the characteristic path length are shown as a function of the sparsity thresholds compared with the matched random networks. (C) The small-worldness is shown as a function of the sparsity thresholds. (D) Global efficiency, (E) local efficiency, and (F) modularity are presented as a function of the sparsity thresholds compared with the matched random networks. Error bars (A, B, D, E, F) correspond to the standard errors of the mean for 1000 comparable random null networks. Error bars in (C) indicate the standard errors in all subjects.

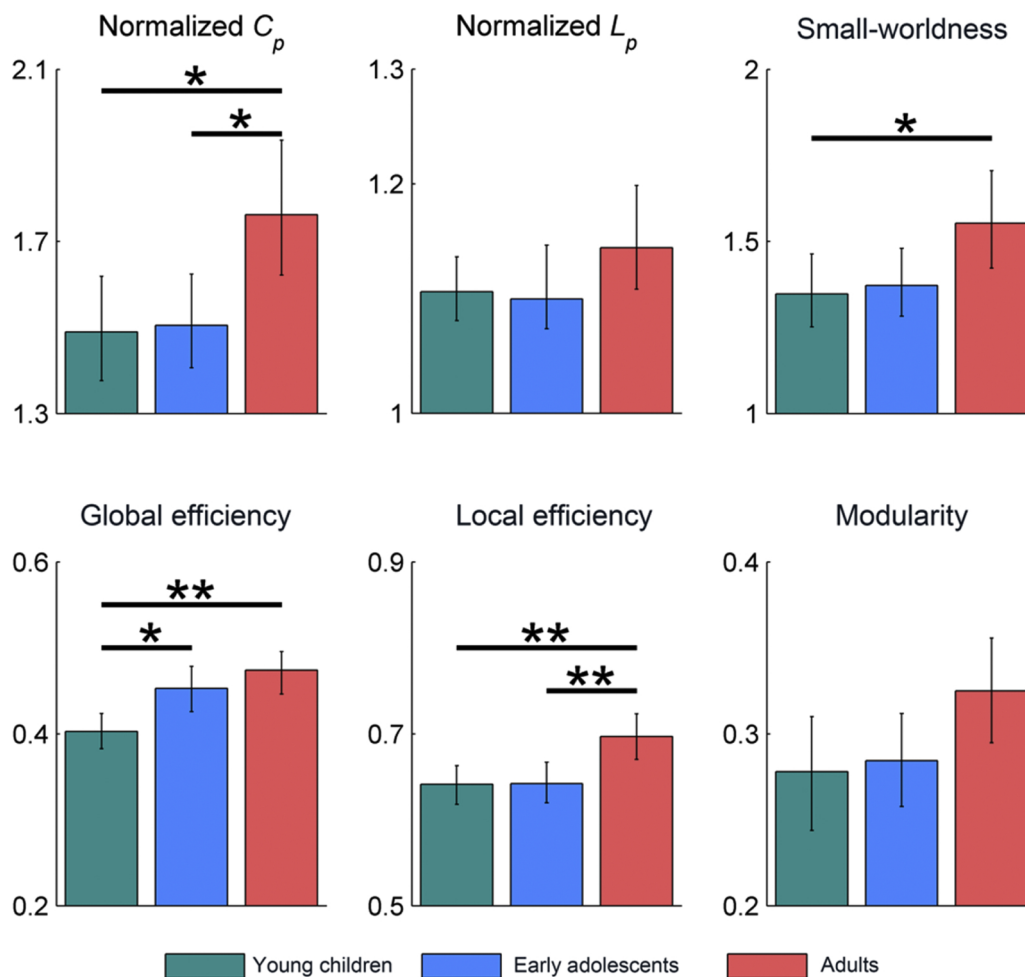


Fig. 5. Group differences in the global network metrics among the three age groups. * $p < 0.05$, ** $p < 0.01$. The error bars indicate bootstrapped 95% confidence intervals. Overlapping confidence intervals suggest a lack of difference.

$p = 0.036$), global efficiency ($F_{(2,87)} = 8.60$, $p = 0.000$) and local efficiency ($F_{(2,87)} = 6.44$, $p = 0.003$). Further statistical analysis indicated that all of these four network measures revealed significant age-related increases during the development from children to adults (*post hoc* tests, $p < 0.05$). Network normalized C_p and local efficiency exhibited significant developmental increases from early adolescents to adults (*post hoc* tests, $p < 0.05$), and global efficiency showed developmental increases from young children to early adolescents (*post hoc* tests, $p < 0.05$). However, no significant age-related changes in normalized L_p and modularity were detected ($p > 0.05$).

3.4. Developmental changes in regional nodal properties and hub distribution

GLM analysis was used to examine developmental changes in the regional nodal parameters. With the nodal degree, significant age-related increases were primarily distributed in the frontal brain region (channel 6) ($p < 0.05$, corrected by FDR correction, Fig. 6A, red spheres), while decreases were in the frontal (channel 21) and parietal (channel 35) areas ($p < 0.05$, corrected by FDR correction, Fig. 6A, blue spheres). With the nodal efficiency, significant age-related increases were primarily distributed in frontal (channels 6 and 9) and occipital regions (channels 42 and 43) ($p < 0.05$, corrected by FDR correction, Fig. 6B, red spheres), and no age-related decrease was found.

The hub distributions of young children, early adolescents, and adults were presented in Figs. 6C (nodal degree) and 6D (nodal

efficiency), respectively. With regional nodal degree as the measurement, four frontal (channels 2, 4, 5, and 11) and one parietal regions (channel 17) are the common hubs for all of the three age groups. Notably, the number of frontal hubs increased from early childhood to adulthood. With regional nodal efficiency as the measurement, three frontal areas in channels 2, 4, and 11 and one parietal region in channel 17 are the common hubs for all of the three age groups. Similar to nodal degree, the number of frontal hubs increased from early childhood to adulthood.

3.5. Validation results

Using the HbR-derived binary brain network, we first evaluated the effects of different network sparsity thresholds (15% and 25%) on the main findings. We found that the main conclusions remained as different network sparsity values were utilized. For example, with network sparsity values at 15% and 25%, the network metrics of normalized clustering coefficient, global efficiency and local efficiency showed increases with development (Fig. 7A and C), and the number of frontal hubs increased from early childhood to adulthood (Fig. 7B and D). These results across different sparsity thresholds (15% vs. 25%) were highly similar to those calculated using the sparsity 20% (Figs. 5 and 6).

Furthermore, we also evaluated the effect of the weighted network analysis strategy on main findings using sparsity threshold 20%. The main conclusions were partially preserved when compared to those obtained from binary network results, e.g., the global normalized C_p significantly increased from young children to adults and from

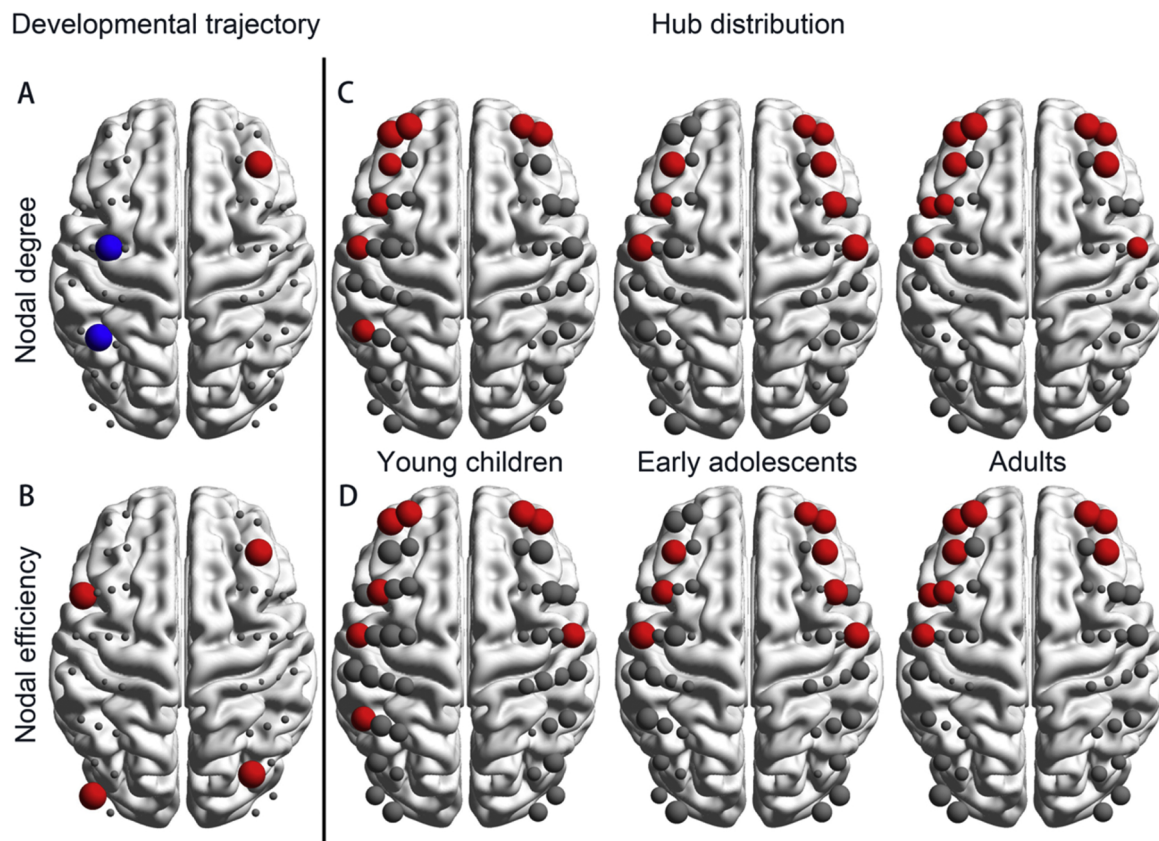


Fig. 6. Development changes in the regional nodal properties and the distributions of hub regions in each age group. (A) The developmental trajectories for significant nodes in nodal degree. (B) The developmental trajectories for significant nodes in nodal efficiency. Regions with significantly linear positive and linear negative correlations are indicated by red and blue spheres, respectively. The significances were set at $p < 0.05$ (corrected by FDR correction). The hubs in each age group are defined as the brain regions with higher values (Mean + SD) in any of (C) node degree and (D) node efficiency. The hubs are shown in red with node sizes that indicate the values in regional nodal properties. (For interpretation of the references to colour in this figure legend, the reader is referred to the web version of this article.)

adolescents to adults (Fig. 8A), as well as the regional nodal hubs were mainly located in the frontal brain regions across these three age groups (Fig. 8B). However, the other network parameters (e.g., global efficiency and local efficiency) showed no significant age effects, which is different from the results derived from binary network.

Finally, using the HbO signals, we examined the effect of different hemoglobin concentration signals on the main findings. Binary network and 20% sparsity thresholds were used to construct the brain network. The results were included in the Supplementary Materials. Specifically, for global network metrics, the HbO-derived normalized clustering coefficient, small-worldness, global efficiency, and modularity significantly decreased, while normalized L_p significantly increased during the development from children to adults (*post hoc* tests, $p < 0.05$) (Fig. S3). Network global efficiency exhibited significant developmental decreases from adolescents to adults (*post hoc* tests, $p < 0.05$). Network local efficiency did not show any age-related changes. For nodal network measures, e.g., the nodal degree, significant age-related increases were primarily distributed in frontal (channels 1, 3, 4, 5, and 6) and occipital (channels 43 and 44) brain regions ($p < 0.05$, corrected by Bonferroni correction, Fig. S4A, red spheres), while decreases were in the frontal (channels 19–22) and parietal (channels 27, 29, 31, and 32) areas ($p < 0.05$, corrected by Bonferroni correction, Fig. S4A, blue spheres). A U-shape developmental trajectory was found in the parietal area (channel 17, a green sphere) during the development from young children to adults (Fig. S4A). With nodal efficiency, significant age-related decreases were primarily distributed in frontal (channels 19–22) and parietal (channels 27, 29–32, and 36) regions ($p < 0.05$, corrected by Bonferroni correction, Fig. S4B, red spheres), and no age-related increase was found. The developmental trajectories of the nodal degree

obtained based on HbR and HbO share some important aspects: the nodal degree increases with age over some frontal nodes, and it decreases over more parietal nodes. Furthermore, the hub distributions for HbO signals retained good similarity to those obtained using HbR, and the number of frontal hubs increased from early childhood to adulthood, irrespective of whether nodal degree or nodal efficiency was adopted for these two concentration signals.

4. Discussion

In this study, we employed rs-fNIRS data and the graph-theory approach to investigate the age-related topological organization of human brain functional connectivity from early childhood and early adolescence to adulthood. The main findings included the following: 1) functional brain networks in the three age groups showed a uniformly comparable economical small-world organization; 2) young children exhibited a decreased global efficiency compared with early adolescents and adults. Young children and early adolescents had lower values than adults in local efficiency; and (3) heterogeneous developmental patterns in nodal topological characteristics were found, for example, right middle frontal gyrus exhibited a significant linear age-related increase with maturation, indicating that increasing cognitive capacity may relate to right middle frontal gyrus. Overall, we observed significant developmental changes in the topological organization of functional networks from early childhood and early adolescence to adulthood. Our results provided an insight into understanding important topological changes occurring in brain functional networks across the two landmark developmental stages from early childhood to early adolescence. These findings are discussed in detail below.

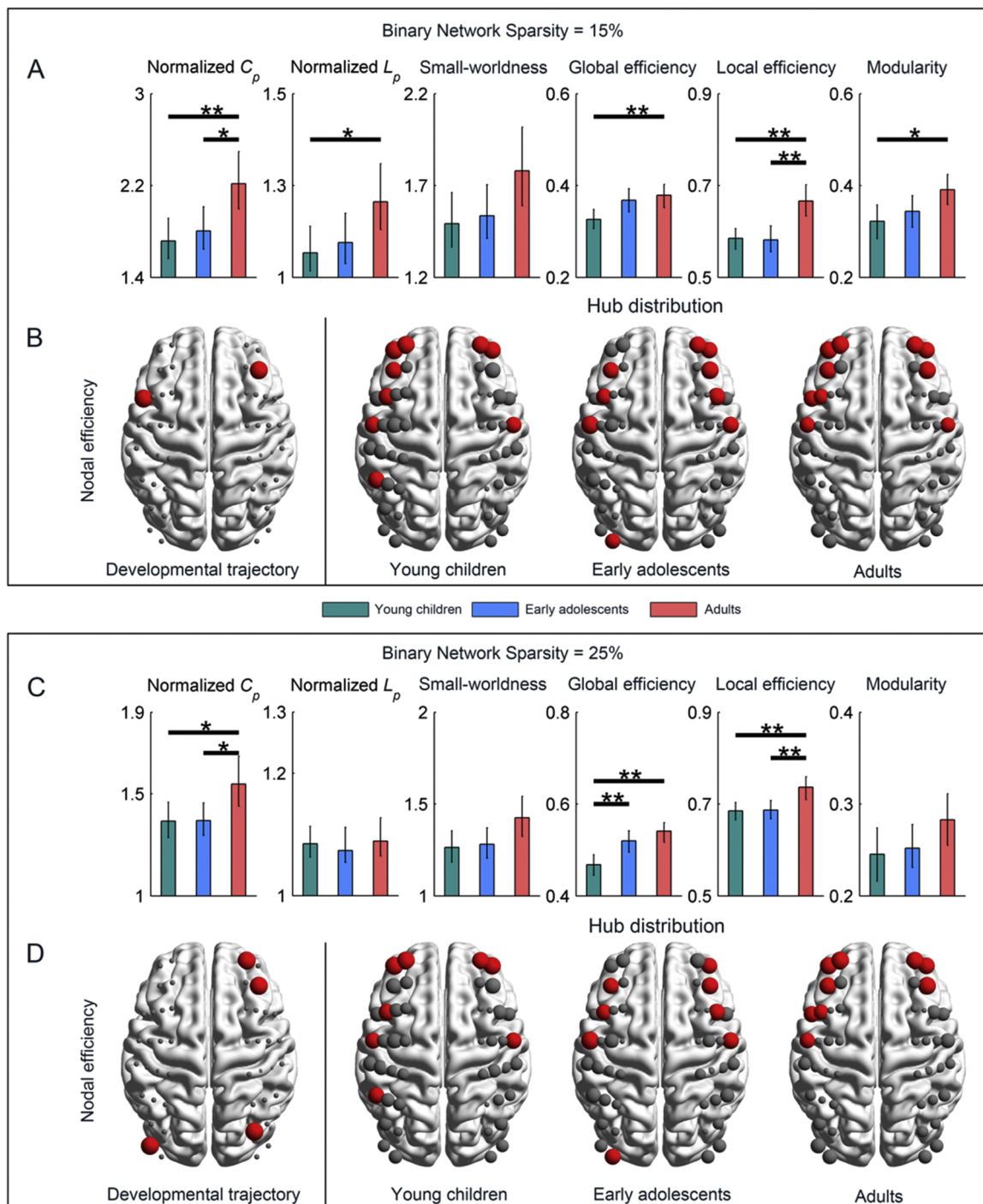


Fig. 7. The effects of different network sparsity thresholds (15% and 25%) on the main findings. Binary networks were used to evaluate the effects.

The economical small-world architecture was consistently identified in the functional brain networks across these three age groups in our study. Brain networks with small-world attributes can offer a topological underpinning for both locally specialized and globally distributed processing (Achard and Bullmore, 2007; Bassett and Bullmore, 2006). Recent studies on structural and functional brain networks indicated that the small-world organization is established in the very early life of the human brain (Gao et al., 2011; Huang et al., 2015; van den Heuvel et al., 2015; Yap et al., 2011). Thus, our results provided further support for findings that the human brain has an efficient functional network organization throughout maturation (Fair et al., 2009; Supekar et al., 2009; Wu et al., 2013).

We also determined that global efficiency significantly increased from young children to early adolescents and adults. This finding is approximately consistent with previous structural MRI studies that reported increases in global efficiency through childhood (i.e., 4.8–11.3 years old) (Khundrakpam et al., 2013), and from early stage of life (e.g., 2 years of age) to adulthood (Dennis et al., 2013; Hagmann et al., 2010; Huang et al., 2015). This increased global efficiency from early childhood to adults may reflect a neurocognitive maturation process in the functional brain networks. The increasing global efficiency in the brain was also confirmed to be significantly positively associated with humans intellectual performance (Li et al., 2009; Stam and van Straaten, 2012; van den Heuvel et al., 2009), which indicates that cognitive

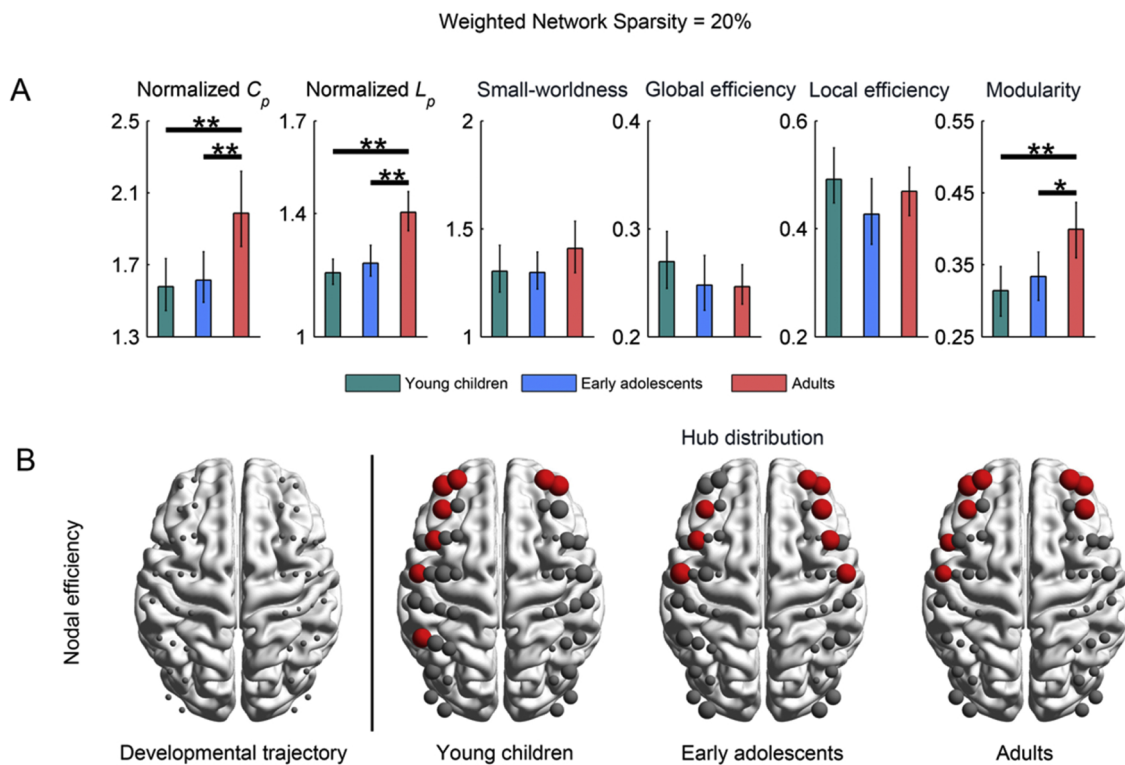


Fig. 8. The effects of weighted network analysis strategy on the main findings. Sparsity threshold of 20% was used to evaluate the effects.

ability is possibly related to how efficiently the global connections of the brain are organized, and how efficiently information can be integrated globally between the different regions of the brain network. However, it is also noted that our findings are not completely compatible with previous fMRI-based imaging studies (Cao et al., 2014; Supekar et al., 2009; Wu et al., 2013) that found no significant difference in network global efficiency across development. Interestingly, the local efficiency obtained from these two modalities (fMRI in previous studies & fNIRS in the current study) preserved some common findings, i.e., the local efficiency exhibited significant increases from young children or adolescents to adults (Cao et al., 2014; Wu et al., 2013). However, Cao et al. and Wu et al. (Cao et al., 2014; Wu et al., 2013) demonstrated a monotonic increase in local efficiency from childhood and adolescence to adulthood, and our study pointed out no significant differences in local efficiency between childhood and adolescence. The higher local efficiency has been suggested to be associated with efficient information processing among topologically nearby neighbors and high error tolerance (Bullmore and Sporns, 2009; He and Evans, 2010). It should also be noted that not all developmental procedures from birth to adulthood are associated with monotonic processes (Chugani et al., 1987). Our results suggested that the functional segregation of human brain networks could undergo a relatively steady development plateau from early childhood to early adolescence rather than a linear increase. Moreover, the human brain in early childhood and early adolescence perhaps does not achieve an optimal network configuration, which may provide a neural basis for nonlinear shifts in behavior across development due to earlier maturation of the limbic structure relative to the less mature top-down prefrontal control region (Casey et al., 2008).

Modularity is quantified by the extent to which the network can be separated into modules, and thus it constitutes a topological organization principle that is related to clustering, which favors specialized or segregated information processing in the brain networks. In our study, modularity was found to remain approximately constant across childhood, adolescence and adulthood, which was consistent with Fair et al.'s study (Fair et al., 2009), but different from Cao et al.'s study that demonstrated a linear decrease in modularity (Cao et al., 2014). This

divergence in the modularity results may be related to the number of the participants and their age range distribution, as well as the network construction methods and different imaging modalities.

For nodal properties of the brain network, linear increases were primarily identified in the frontal cortex, particularly the middle frontal gyrus (Fig. 6). These frontal cortices have been suggested to mature much later and be associated with increasing cognitive capacity during childhood (Casey et al., 2000). By contrast, nodes with linear decreases in nodal properties were primarily in the parietal cortex and precentral gyrus (Fig. 6). These nodes, related to the primary somatosensory region, gradually play a less important role in the whole brain due to their early development. These results demonstrated that many cognitive abilities experience rapid development from early childhood to early adolescence, but their network connection configuration remains in an immature state compared with adults (Bunge et al., 2002; Casey et al., 2008).

Hub regions in functional brain networks are believed to play a central role in global information integration between parallel and distributed networks (Hwang et al., 2013). In the adult brain, functional cortical hubs include the medial prefrontal cortex, posterior cingulate cortex (PCC), precuneus, inferior parietal lobule, and medial temporal cortex (Buckner et al., 2009). In our study, the functional hubs in the three age groups were also predominately located in the frontal and parietal lobes (Fig. 6), which may result from increases in the frontal-parietal hub-hub structural connectivity over time (Baker et al., 2015). Additionally, the number of frontal hubs increased from early childhood to adulthood, indicating that frontal hubs may take a few decades to form, and corresponds well with maturation from concrete operational thinking in childhood to formal operations in adolescence.

In the present study, the main results were presented by analyzing HbR signals. When considering HbO signals, we found that some global network metrics (e.g., normalized clustering coefficient and global efficiency) showed different developmental patterns between HbR and HbO signals. Although our previous studies (Niu and He, 2014; Niu et al., 2013; Niu et al., 2012) have demonstrated that both HbO and HbR signals can be used to characterize topological organization of

intrinsic functional brain networks, the quantitative network parameters differ significantly due to different concentration signals. Here, we further found that the developmental patterns in topological organization displayed obvious difference between these two concentration signals. The discrepancies may be attributable to that different hemoglobin concentration signals reflect different nature in hemodynamic responses to transient neural activity and/or the difference in signal-to-noise ratio in the rs-fNIRS measurements (Gagnon et al., 2012; Niu et al., 2013; White et al., 2009). Because HbO signals reflect regional cerebral blood flow changes whereas HbR signals are generated through oxygen utilization in cerebral tissue, HbO signals are generally vulnerable to various noise components compared to HbR signals (Kirilina et al., 2012; Strangman et al., 2002). Furthermore, our previous study has proved that HbR signals provide better network metric reliability than HbO signals (Niu et al., 2013). Therefore, the noise in the concentration signals could lead to distinct effects on the present results. Additionally, the fMRI BOLD signal has been proposed to originate from the paramagnetic properties of HbR signals (Buxton et al., 1998; Ogawa et al., 1993), which follows the BOLD signal more closely than HbO signals (Huppert et al., 2006; Kleinschmidt et al., 1996; Toronov et al., 2003). Thus, we assumed that the current results derived from HbR signals may be comparable to previous fMRI evidence.

There are several issues in the current study that should be addressed. First, head motion artifacts and systematic physiological superficial noise are two important noise sources in fNIRS signals. In our study, we adopted the ICA method to reduce the influence from these two noise sources. However, ICA belongs to blind source separation, which makes it lack an explicit physiological explanation for identified components. In addition, blind source separation also gives rise to difficulties of completely identifying and removing noise components from recorded brain activity signals. This issue is challenging in resting-state fNIRS studies and should be studied carefully in the future. Second, the significant developmental trend in the nodal properties found in this study could be conservative, because it is not ideal to use GLM to examine the developmental effects for non-continuous age ranges. Another concern is that we utilized the same probe geometry for data collection on all participants. It is known that head circumference constitutes an important index to characterize brain development for children. For example, the head circumference in children should be approximately 50 cm (e.g., approximately 5 years old), whereas that in adolescents should be relatively much larger than in children, but similar to that in adults (approximately 54–58 cm). As such, it remains interesting whether brain signals from different population groups recorded brain activity information at the same or similar regions of the human cerebral cortex across groups. Finally, this study is a cross-sectional developmental study in which individual variations existed and may affect the current main results. Future studies with longitudinal resting fNIRS data collection are required to further validate the findings observed in this study.

5. Conclusion

We observed a stable small-world organization in functional brain networks derived from rs-fNIRS and significant developmental effects on both global and regional nodal properties from early childhood to adulthood. In particular, we determined that young children had a significantly lower global efficiency than early adolescents and adults, which revealed that the integration of the distributed networks strengthens across developmental stages underlying cognitive development. In addition, the local efficiency of young children and adolescents was significantly lower than that of adults, while there was no difference between these two younger groups. This finding revealed that functional segregation remained relatively stable from early childhood to early adolescence, and the human brain in these developmental periods did not have an optimal network configuration, like adults. Furthermore, we found heterogeneous developmental patterns

in regional nodal properties in various brain regions, such as the linear increased nodal properties in the frontal cortex, indicating increasing cognitive capacity over development. Collectively, our results demonstrated that there were significant topological changes in functional network organization during these two critical developmental stages, and provided a novel insight into understanding the subtle changes in brain functional networks across development.

Conflict of Interest

None

Acknowledgments

We wish to thank Shujie Geng for helping with data acquisition, and Zhaojun Zhu and Miao Cao for assistance with Matlab programming. This study is supported by the Natural Science Foundation of China (Grant nos. 81571755, 31521063, 81761148026, 81201122), the Beijing Municipal Science and Technology Commission (Z151100003915122), and the Open Research Fund of the State Key Laboratory of Cognitive Neuroscience and Learning.

Appendix A. Supplementary data

Supplementary data associated with this article can be found, in the online version, at <https://doi.org/10.1016/j.dcn.2018.03.003>.

References

- Achard, S., Bullmore, E., 2007. Efficiency and cost of economical brain functional networks. *PLoS Comput. Biol.* 3 (2), e17. <http://dx.doi.org/10.1371/journal.pcbi.0030017>.
- Baker, S.T.E., Lubman, D.I., Yucel, M., Allen, N.B., Whittle, S., Fulcher, B.D., Fornito, A., 2015. Developmental changes in brain network hub connectivity in late adolescence. *J. Neurosci.* 35 (24), 9078–9087. <http://dx.doi.org/10.1523/jneurosci.5043-14.2015>.
- Bassett, D.S., Bullmore, E.T., 2006. Small-world brain networks. *Neuroscientist* 12 (6), 512–523. <http://dx.doi.org/10.1177/1073858406293182>.
- Bassett, D.S., Bullmore, E., Verchinski, B.A., Mattay, V.S., Weinberger, D.R., Meyer-Lindenberg, A., 2008. Hierarchical organization of human cortical networks in health and schizophrenia. *J. Neurosci.* 28 (37), 9239–9248. <http://dx.doi.org/10.1523/JNEUROSCI.1929-08.2008>.
- Bedard, A.C., Nichols, S., Barbosa, J.A., Schachar, R., Logan, G.D., Tannock, R., 2002. The development of selective inhibitory control across the life span. *Dev. Neuropsychol.* 21 (1), 93–111. http://dx.doi.org/10.1207/S15326942DN2101_5.
- Benjamini, Y., Hochberg, Y., 1995. Controlling the false discovery rate – a practical and powerful approach to multiple testing. *J. R. Stat. Soc. Ser. B (Methodological)* 57 (1), 289–300.
- Biswal, B., Yetkin, F.Z., Haughton, V.M., Hyde, J.S., 1995. Functional connectivity in the motor cortex of resting human brain using echo-planar mri. *Magn. Reson. Med.* 34 (4), 537–541. <http://dx.doi.org/10.1002/mrm.1910340409>.
- Brocki, K.C., Bohlin, G., 2004. Executive functions in children aged 6 to 13: a dimensional and developmental study. *Dev. Neuropsychol.* 26 (2), 571–593. http://dx.doi.org/10.1207/s15326942dn2602_3.
- Buckner, R.L., Sepulcre, J., Talukdar, T., Krienen, F.M., Liu, H., Hedden, T., Johnson, K.A., 2009. Cortical hubs revealed by intrinsic functional connectivity: mapping, assessment of stability, and relation to Alzheimer's disease. *J. Neurosci.* 29 (6), 1860–1873. <http://dx.doi.org/10.1523/jneurosci.5062-08.2009>.
- Bullmore, E.T., Sporns, O., 2009. Complex brain networks: graph theoretical analysis of structural and functional systems. *Nat. Rev. Neurosci.* 10 (3), 186–198. <http://dx.doi.org/10.1038/nrn2575>.
- Bunge, S.A., Wright, S.B., 2007. Neurodevelopmental changes in working memory and cognitive control. *Curr. Opin. Neurobiol.* 17 (2), 243–250. <http://dx.doi.org/10.1016/j.conb.2007.02.005>.
- Bunge, S.A., Dudukovic, N.M., Thomason, M.E., Vaidya, C.J., Gabrieli, J.D., 2002. Immature frontal lobe contributions to cognitive control in children: evidence from fMRI. *Neuron* 33 (2), 301–311.
- Buxton, R.B., Wong, E.C., Frank, L.R., 1998. Dynamics of blood flow and oxygenation changes during brain activation: the balloon model. *Magn. Reson. Med.* 39 (6), 855–864.
- Cao, M., Wang, J.H., Dai, Z.J., Cao, X.Y., Jiang, L.L., Fan, F.M., He, Y., 2014. Topological organization of the human brain functional connectome across the lifespan. *Dev. Cogn. Neurosci.* 7, 76–93. <http://dx.doi.org/10.1016/j.dcn.2013.11.004>.
- Casey, B.J., Giedd, J.N., Thomas, K.M., 2000. Structural and functional brain development and its relation to cognitive development. *Biol. Psychol.* 54 (1–3), 241–257. [http://dx.doi.org/10.1016/s0301-0511\(00\)00058-2](http://dx.doi.org/10.1016/s0301-0511(00)00058-2).
- Casey, B.J., Getz, S., Galvan, A., 2008. The adolescent brain. *Dev. Rev.* 28 (1), 62–77.

- <http://dx.doi.org/10.1016/j.dr.2007.08.003>.
- Chugani, H.T., Phelps, M.E., Mazziotta, J.C., 1987. Positron emission tomography study of human brain functional development. *Ann. Neurol.* 22 (4), 487–497. <http://dx.doi.org/10.1002/ana.410220408>.
- Collin, G., van den Heuvel, M.P., 2013. The ontogeny of the human connectome: development and dynamic changes of brain connectivity across the life span. *Neuroscientist* 19 (6), 616–628. <http://dx.doi.org/10.1177/1073858413503712>.
- Cope, M., Delpy, D.T., 1988. System for long-term measurement of cerebral blood and tissue oxygenation on newborn-infants by near-infrared trans-illumination. *Med. Biol. Eng. Comput.* 26 (3), 289–294. <http://dx.doi.org/10.1007/bf02447083>.
- Davidson, M.C., Amso, D., Anderson, L.C., Diamond, A., 2006. Development of cognitive control and executive functions from 4 to 13 years: evidence from manipulations of memory, inhibition, and task switching. *Neuropsychologia* 44 (11), 2037–2078. <http://dx.doi.org/10.1016/j.neuropsychologia.2006.02.006>.
- Dennis, E.L., Jahanshad, N., McMahon, K.L., de Zubicaray, G.I., Martin, N.G., Hickie, I.B., Thompson, P.M., 2013. Development of brain structural connectivity between ages 12 and 30: A 4-Tesla diffusion imaging study in 439 adolescents and adults. *Neuroimage* 64, 671–684. <http://dx.doi.org/10.1016/j.neuroimage.2012.09.004>.
- Ernst, M., Mueller, S.C., 2008. The adolescent brain: insights from functional neuroimaging research. *Dev. Neurobiol.* 68 (6), 729–743. <http://dx.doi.org/10.1002/dneu.20615>.
- Fair, D.A., Cohen, A.L., Power, J.D., Dosenbach, N.U.F., Church, J.A., Miezin, F.M., Petersen, S.E., 2009. Functional brain networks develop from a local to distributed organization. *PLoS Comput. Biol.* 5 (5). <http://dx.doi.org/10.1371/journal.pcbi.1000381>.
- Fan, Y., Shi, F., Smith, J.K., Lin, W., Gilmore, J.H., Shen, D.G., 2011. Brain anatomical networks in early human brain development. *Neuroimage* 54 (3), 1862–1871. <http://dx.doi.org/10.1016/j.neuroimage.2010.07.025>.
- Fox, M.D., Zhang, D., Snyder, A.Z., Raichle, M.E., 2009. The global signal and observed anticorrelated resting state brain networks. *J. Neurophysiol.* 101 (6), 3270–3283. <http://dx.doi.org/10.1152/jn.90777.2008>.
- Gagnon, L., Yucel, M.A., Dehaes, M., Cooper, R.J., Perdue, K.L., Selb, J., Boas, D.A., 2012. Quantification of the cortical contribution to the NIRS signal over the motor cortex using concurrent NIRS-fMRI measurements. *Neuroimage* 59 (4), 3933–3940. <http://dx.doi.org/10.1016/j.neuroimage.2011.10.054>.
- Gao, W., Gilmore, J.H., Giovanello, K.S., Smith, J.K., Shen, D., Zhu, H., Lin, W., 2011. Temporal and spatial evolution of brain network topology during the first two years of life. *PLoS One* 6 (9), e25278. <http://dx.doi.org/10.1371/journal.pone.0025278>.
- Garrett, D.D., Kovacevic, N., McIntosh, A.R., Grady, C.L., 2013. The modulation of BOLD variability between cognitive states varies by age and processing speed. *Cereb. Cortex* 23 (3), 684–693. <http://dx.doi.org/10.1093/cercor/bhs055>.
- Gathercole, S.E., Pickering, S.J., Ambridge, B., Wearing, H., 2004. The structure of working memory from 4 to 15 years of age. *Dev. Psychol.* 40 (2), 177–190. <http://dx.doi.org/10.1037/0012-1649.40.2.177>.
- Giedd, J.N., Blumenthal, J., Jeffries, N.O., Castellanos, F.X., Liu, H., Zijdenbos, A., Rapoport, J.L., 1999. Brain development during childhood and adolescence: a longitudinal MRI study. *Nat. Neurosci.* 2 (10), 861–863. <http://dx.doi.org/10.1038/13158>.
- Hagmann, P., Sporns, O., Madan, N., Cammoun, L., Pienaar, R., Wedeen, V.J., Grant, P.E., 2010. White matter maturation reshapes structural connectivity in the late developing human brain. *Proc. Natl. Acad. Sci. U. S. A.* 107 (44), 19067–19072. <http://dx.doi.org/10.1073/pnas.1009073107>.
- Hagmann, P., Grant, P.E., Fair, D.A., 2012. MR connectomics: a conceptual framework for studying the developing brain. *Front. Syst. Neurosci.* 6, 43. <http://dx.doi.org/10.3389/fnsys.2012.00043>.
- He, Y., Evans, A., 2010. Graph theoretical modeling of brain connectivity. *Curr. Opin. Neurol.* 23 (4), 341–350. <http://dx.doi.org/10.1097/WCO.0b013e3181933aa567>.
- Huang, H., Shu, N., Mishra, V., Jeon, T., Chalal, L., Wang, Z.Y.J., He, Y., 2015. Development of human brain structural networks through infancy and childhood. *Cereb. Cortex* 25 (5), 1389–1404. <http://dx.doi.org/10.1093/cercor/bht335>.
- Huppert, T.J., Hoge, R.D., Diamond, S.G., Franceschini, M.A., Boas, D.A., 2006. A temporal comparison of BOLD, ASL, and NIRS hemodynamic responses to motor stimuli in adult humans. *Neuroimage* 29 (2), 368–382. <http://dx.doi.org/10.1016/j.neuroimage.2005.08.065>.
- Hurvich, C.M., Tsai, C.L., 1989. Regression and time-series model selection in small samples. *Biometrika* 76 (2), 297–307.
- Hwang, K., Hallquist, M.N., Luna, B., 2013. The development of hub architecture in the human functional brain network. *Cereb. Cortex* 23 (10), 2380–2393. <http://dx.doi.org/10.1093/cercor/bhs227>.
- Khundrakpam, B.S., Reid, A., Brauer, J., Carbonell, F., Lewis, J., Ameis, S., Brain Development Cooperative, G., 2013. Developmental changes in organization of structural brain networks. *Cereb. Cortex* 23 (9), 2072–2085. <http://dx.doi.org/10.1093/cercor/bhs187>.
- Kirilina, E., Jelzow, A., Heine, A., Niessing, M., Wabnitz, H., Bruhl, R., Tachtsidis, I., 2012. The physiological origin of task-evoked systemic artefacts in functional near infrared spectroscopy. *Neuroimage* 61 (1), 70–81. <http://dx.doi.org/10.1016/j.neuroimage.2012.02.074>.
- Kleinschmidt, A., Obrig, H., Requardt, M., Merboldt, K.D., Dirnagl, U., Villringer, A., Frahm, J., 1996. Simultaneous recording of cerebral blood oxygenation changes during human brain activation by magnetic resonance imaging and near-infrared spectroscopy. *J. Cereb. Blood Flow Metab.* 16 (5), 817–826. <http://dx.doi.org/10.1097/00004647-199609000-00006>.
- Kohno, S., Miyai, I., Seiyama, A., Oda, I., Ishikawa, A., Tsuneishi, S., Shimizu, K., 2007. Removal of the skin blood flow artifact in functional near-infrared spectroscopic imaging data through independent component analysis. *J. Biomed. Opt.* 12 (6), 062111. <http://dx.doi.org/10.1117/1.2814249>.
- Kovelman, I., Shalinsky, M.H., Berens, M.S., Petitto, L.A., 2008. Shining new light on the brain's bilingual signature: a functional Near Infrared Spectroscopy investigation of semantic processing. *Neuroimage* 39 (3), 1457–1471. <http://dx.doi.org/10.1016/j.neuroimage.2007.10.017>.
- Kovelman, I., Shalinsky, M.H., White, K.S., Schmitt, S.N., Berens, M.S., Paymer, N., Petitto, L.A., 2009. Dual language use in sign-speech bimodal bilinguals: fNIRS brain-imaging evidence. *Brain Lang.* 109 (2–3), 112–123. <http://dx.doi.org/10.1016/j.bandl.2008.09.008>.
- Latora, V., Marchiori, M., 2001. Efficient behavior of small-world networks. *Phys. Rev. Lett.* 87 (19), 198701. <http://dx.doi.org/10.1103/PhysRevLett.87.198701>.
- Latora, V., Marchiori, M., 2003. Economic small-world behavior in weighted networks. *Eur. Phys. J. B - Cond. Mat. Complex Syst.* V32 (2), 249–263.
- Li, Y., Liu, Y., Li, J., Qin, W., Li, K., Yu, C., Jiang, T., 2009. Brain anatomical network and intelligence. *PLoS Comput. Biol.* 5 (5), e1000395. <http://dx.doi.org/10.1371/journal.pcbi.1000395>.
- Lloyd-Fox, S., Blasi, A., Elwell, C.E., 2010. Illuminating the developing brain: the past, present and future of functional near infrared spectroscopy. *Neurosci. Biobehav. Rev.* 34 (3), 269–284. <http://dx.doi.org/10.1016/j.neubiorev.2009.07.008>.
- Murphy, K., Birn, R.M., Handwerker, D.A., Jones, T.B., Bandettini, P.A., 2009. The impact of global signal regression on resting state correlations: are anti-correlated networks introduced? *Neuroimage* 44 (3), 893–905. <http://dx.doi.org/10.1016/j.neuroimage.2008.09.036>.
- Newman, M.E., 2006. Modularity and community structure in networks. *Proc. Natl. Acad. Sci. U. S. A.* 103 (23), 8577–8582. <http://dx.doi.org/10.1073/pnas.0601602103>.
- Niu, He, Y., 2014. Resting-state functional brain connectivity: lessons from functional near-infrared spectroscopy. *Neuroscientist* 20 (2), 173–188. <http://dx.doi.org/10.1177/1073858413502707>.
- Niu, Wang, J., Zhao, T., Shu, N., He, Y., 2012. Revealing topological organization of human brain functional networks with resting-state functional near infrared spectroscopy. *PLoS One* 7 (9), e45771. <http://dx.doi.org/10.1371/journal.pone.0045771>.
- Niu, Li, Z., Liao, X., Wang, J., Zhao, T., Shu, N., He, Y., 2013. Test-retest reliability of graph metrics in functional brain networks: a resting-state fNIRS study. *PLoS One* 8 (9), e72425. <http://dx.doi.org/10.1371/journal.pone.0072425>.
- Ogawa, S., Menon, R.S., Tank, D.W., Kim, S.G., Merkle, H., Ellermann, J.M., Ugurbil, K., 1993. Functional brain mapping by blood oxygenation level-dependent contrast magnetic-resonance-imaging - a comparison of signal characteristics with a biophysical model. *Biophys. J.* 64 (3), 803–812.
- Oldfield, R.C., 1971. The assessment and analysis of handedness: the edinburgh inventory. *Neuropsychologia* 9 (1), 97–113.
- Piaget, J., 1999. The stages of the intellectual development of the child. In: Slater, A. (Ed.), *The Blackwell Reader in Developmental Psychology*. Blackwell Publishing Ltd, Malden, pp. 35–42.
- Rubinow, M., Sporns, O., 2010. Complex network measures of brain connectivity: uses and interpretations. *Neuroimage* 52 (3), 1059–1069. <http://dx.doi.org/10.1016/j.neuroimage.2009.10.003>.
- Sasai, S., Homae, F., Watanabe, H., Sasaki, A.T., Tanabe, H.C., Sadato, N., Taga, G., 2012. A NIRS-fMRI study of resting state network. *Neuroimage* 63 (1), 179–193. <http://dx.doi.org/10.1016/j.neuroimage.2012.06.011>.
- Schneider, W., Ornstein, P.A., 2015. The development of children's memory. *Child Dev.* 9 (3), 190–195. <http://dx.doi.org/10.1111/cdep.12129>.
- Sowell, E.R., Peterson, B.S., Thompson, P.M., Welcome, S.E., Henkenius, A.L., Toga, A.W., 2003. Mapping cortical change across the human life span. *Nat. Neurosci.* 6 (3), 309–315. <http://dx.doi.org/10.1038/nn1008>.
- Sporns, O., Zwi, J.D., 2004. The small world of the cerebral cortex. *Neuroinformatics* 2 (2), 145–162. <http://dx.doi.org/10.1385/NI:2:2:145>.
- Stam, C.J., van Straaten, E.C., 2012. The organization of physiological brain networks. *Clin. Neurophysiol.* 123 (6), 1067–1087. <http://dx.doi.org/10.1016/j.clinph.2012.01.011>.
- Stam, C.J., Jones, B.F., Nolte, G., Breakspear, M., Scheltens, P., 2007. Small-world networks and functional connectivity in Alzheimer's disease. *Cereb. Cortex* 17 (1), 92–99.
- Strangman, G., Culver, J.P., Thompson, J.H., Boas, D.A., 2002. A quantitative comparison of simultaneous BOLD fMRI and NIRS recordings during functional brain activation. *Neuroimage* 17 (2), 719–731.
- Supekar, K., Musen, M., Menon, V., 2009. Development of large-scale functional brain networks in children. *PLoS Biol.* 7 (7). <http://dx.doi.org/10.1371/journal.pbio.1000157>.
- Toronov, V., Walker, S., Gupta, R., Choi, J.H., Gratton, E., Hueber, D., Webb, A., 2003. The roles of changes in deoxyhemoglobin concentration and regional cerebral blood volume in the fMRI BOLD signal. *Neuroimage* 19 (4), 1521–1531.
- Tzourio-Mazoyer, N., Landeau, B., Papathanassiou, D., Crivello, F., Etard, O., Delcroix, N., Joliot, M., 2002. Automated anatomical labeling of activations in SPM using a macroscopic anatomical parcellation of the MNI MRI single-subject brain. *Neuroimage* 15 (1), 273–289.
- Uehara, T., Yamasaki, T., Okamoto, T., Koike, T., Kan, S., Miyachi, S., Tobimatsu, S., 2014. Efficiency of a small-world brain network depends on consciousness level: a resting-state fMRI study. *Cereb. Cortex* 24 (6), 1529–1539. <http://dx.doi.org/10.1093/cercor/bht004>.
- van den Heuvel, M.P., Stam, C.J., Kahn, R.S., Hulshoff Pol, H.E., 2009. Efficiency of functional brain networks and intellectual performance. *J. Neurosci.* 29 (23), 7619–7624. <http://dx.doi.org/10.1523/JNEUROSCI.1443-09.2009>.
- van den Heuvel, M.P., Kersbergen, K.J., de Reus, M.A., Keunen, K., Kahn, R.S., Groenendaal, F., Benders, M., 2015. The neonatal connectome during preterm brain development. *Cereb. Cortex* 25 (9), 3000–3013. <http://dx.doi.org/10.1093/cercor/bhu095>.
- Vertes, P.E., Bullmore, E.T., 2015. Annual research review: growth connectomics – the

- organization and reorganization of brain networks during normal and abnormal development. *J. Child Psychol. Psychiatry* 56 (3), 299–320. <http://dx.doi.org/10.1111/jcpp.12365>.
- Wang, J., Wang, X., Xia, M., Liao, X., Evans, A., He, Y., 2015. GREYNA: a graph theoretical network analysis toolbox for imaging connectomics. *Front. Hum. Neurosci.* 9, 386. <http://dx.doi.org/10.3389/fnhum.2015.00386>.
- Watts, Strogatz, 1998. Collective dynamics of ‘small-world’ networks. *Nature* 393 (6684), 440–442.
- White, B.R., Snyder, A.Z., Cohen, A.L., Petersen, S.E., Raichle, M.E., Schlaggar, B.L., Culver, J.P., 2009. Resting-state functional connectivity in the human brain revealed with diffuse optical tomography. *Neuroimage* 47 (1), 148–156. <http://dx.doi.org/10.1016/j.neuroimage.2009.03.058>.
- Williams, B.R., Ponesse, J.S., Schachar, R.J., Logan, G.D., Tannock, R., 1999. Development of inhibitory control across the life span. *Dev. Psychol.* 35 (1), 205–213.
- Wu, K., Taki, Y., Sato, K., Hashizume, H., Sassa, Y., Takeuchi, H., Fukuda, H., 2013. Topological organization of functional brain networks in healthy children: differences in relation to age, sex, and intelligence. *PLoS One* 8 (2). <http://dx.doi.org/10.1371/journal.pone.0055347>.
- Xu, J., Liu, X., Zhang, J., Li, Z., Wang, X., Fang, F., Niu, H., 2015. FC-NIRS: a functional connectivity analysis tool for near-infrared spectroscopy data. *BioMed Res. Int.* 2015, 248724. <http://dx.doi.org/10.1155/2015/248724>.
- Yap, P.T., Fan, Y., Chen, Y., Gilmore, J.H., Lin, W., Shen, D., 2011. Development trends of white matter connectivity in the first years of life. *PLoS One* 6 (9), e24678. <http://dx.doi.org/10.1371/journal.pone.0024678>.
- Zhang, H., Zhang, Y.J., Lu, C.M., Ma, S.Y., Zang, Y.F., Zhu, C.Z., 2010. Functional connectivity as revealed by independent component analysis of resting-state fNIRS measurements. *Neuroimage* 51 (3), 1150–1161. <http://dx.doi.org/10.1016/j.neuroimage.2010.02.080>.